





# Slope stability assessment of Ramche and Dhaibung landslides in Central Nepal using geological, geophysical, and geotechnical approaches

Ashok SIGDEL<sup>1,\*</sup> , Pramod DHAKAL<sup>2</sup> , Champak Babu SILWAL<sup>1</sup> , Subash ACHARYA<sup>1</sup> 

<sup>1</sup> Department of Geology, Tri-Chandra Multiple Campus, Tribhuvan University, Ghantaghar, Kathmandu, 44600, Nepal

<sup>2</sup> Department of Electricity Development, Naxal, Kathmandu, Nepal

**Abstract:** The Ramche and Dhaibung landslides, located along Nepal's Pasang Lhamu Highway and Jibjibe route, represent persistent slope instability hazards that threaten local infrastructure and settlements. This study integrates geomorphological, geological, geophysical, and geotechnical approaches to investigate the failure mechanisms and stability conditions of these landslides. Detailed field mapping and satellite image interpretation revealed ongoing mass movement characterized by active erosional gullies, surface deformation, and loose colluvial deposits. Subsurface investigations using Electrical Resistivity Tomography (ERT) identified key geoelectrical contrasts, with low-resistivity zones corresponding to saturated, clay-rich or fractured zones and high-resistivity zones linked to dry, coarse colluvium. These discontinuities indicate weak structural layers and potential slip surfaces at depths of 15–20 metres. Geotechnical tests confirmed that the slope materials comprise poorly graded, low to medium plasticity soils with low cohesion and strength. Mineralogical analysis (XRD) revealed quartz as the dominant mineral and an absence of expansive clay minerals, suggesting that slope failure is primarily driven by hydrological factors rather than swelling clays. Slope stability analysis using the Limit Equilibrium Method indicated that both landslides are stable under dry conditions but become unstable when saturated, with safety factors dropping below 1.0. Additionally, seismic loading scenarios further reduce slope stability, highlighting the compounded risk during the monsoon season. While both sites share similar geological characteristics, the Ramche landslide is more vulnerable due to deeper tension cracks and greater hydrological influence, whereas Dhaibung presents a higher risk of debris flow during rainfall due to its gully-dominated terrain. The study underscores the critical role of rainfall infiltration, weak lithology, and structural discontinuities in driving slope instability, providing a comprehensive understanding essential for landslide hazard mitigation in mountainous terrains.

**Key words:** Ramche landslide, Dhaibung landslide, engineering geology, Electrical Re-

\*corresponding author, e-mail: ashok.sigdel@trc.tu.edu.np

sistivity Tomography (ERT), geotechnical properties, clay mineralogy, Limit Equilibrium Method (LEM)

## 1. Introduction

Landslides are among the most significant natural hazards worldwide, particularly in regions with weak rock formations and steep slopes. Their prevalence is especially pronounced in mountainous terrains, where geological and geomorphological factors collectively contribute to slope instability (Gerrard, 1994). Nepal, situated in the central Himalayas, is highly susceptible to landslides due to its fragile geological structure and pronounced topographical relief (Dangol, 2006). The steep slopes and compact north-south expanse of Nepal create an environment conducive to frequent landslide occurrences and associated erosional activities (Hasegawa et al., 2009).

The primary drivers of slope instability in the Nepalese Himalayas include weak and highly deformed geological formations, often characterized by thrusts, faults, and folds (Upreti, 2001). Extensive research has highlighted the crucial role of geological and geomorphological factors in triggering landslides (Delmonaco et al., 2005; Chigira and Yagi, 2006; Nakano et al., 2016; Kumar et al., 2019; Borrelli et al., 2018; Lupiano et al., 2019; Segoni et al., 2020; Nugraha et al., 2015; Sigdel and Adhikari, 2020a; Lahai et al., 2021). In addition to these natural factors, human activities such as deforestation, improper land-use practices, and slope modifications due to infrastructure development further exacerbate the risk of landslides (Skilodimou et al., 2018; Cui et al., 2023; Jin et al., 2024). Moreover, external triggers such as heavy rainfall and seismic activity significantly heighten the likelihood of slope failures in these regions (Upreti and Dhital, 1996; Dahal and Hasegawa, 2008; Dahal, 2015; Sassa et al., 2007; Muñoz-Torrero Manchado et al., 2021; Keefer, 2002).

Several critical factors influence slope stability, including elevation, geotechnical properties of rocks and soils, weathering intensity, soil thickness, slope aspect, and groundwater dynamics (Bhandari and Dhakal, 2018). Historical landslide events, such as the Trishuli River disaster of 1985 and the devastating 2015 Gorkha earthquake (Mw 7.8), underscore the region's vulnerability to mass wasting processes (Galay, 1987; Xu et al., 2017; Guo et al., 2022). The aftermath of the 2015 earthquake alone resulted in over 1,400

landslides along key transportation corridors, including the Pasang Lhamu Highway, posing a significant threat to local communities and infrastructure (Xu *et al.*, 2017; Pokharel and Thapa, 2019; Williams *et al.*, 2018).

Within this high-risk Himalayan landscape, the Ramche and Dhaibung landslides in Rasuwa District, central Nepal, exemplify the persistent geo-hazard challenges threatening local communities and critical road infrastructure. The Ramche landslide, first triggered in 1983 and catastrophically reactivated in 2003, continues to endanger Polchet village, particularly during the monsoon season (Ghimire *et al.*, 2008). Previous investigations at Ramche have primarily focused on landslide inventories (K.C. *et al.*, 2018), characterization, and GIS or satellite image-based analyses (Xu *et al.*, 2017), rainfall thresholds and shallow landslide dynamics (Guo *et al.*, 2022). While these studies provide valuable insights, they lack detailed geotechnical, geophysical, and slope stability modelling necessary for a comprehensive hazard assessment.

In contrast, the Dhaibung landslide also known as the Dhobi Khola or Dandagumba landslide remains largely unstudied despite its recurrent activity and direct threat to nearby settlements (Nepal Red Cross Society, 2003). Both Ramche and Dhaibung were significantly affected by the 2015 Gorkha earthquake (Mw 7.8), which altered slope conditions and further heightened their susceptibility to failure. A comprehensive investigation integrating geological, geomorphological, geophysical, and geotechnical parameters for slope stability modelling remains absent for both sites. Revisiting Ramche, alongside the first in-depth study of Dhaibung, provides a unique opportunity to conduct a comparison along the same road corridor under similar climatic condition but differing lithological and structural settings. Such an integrated, multidisciplinary approach will not only bridge existing knowledge gaps but also generate site-specific insights that can inform effective stabilization measures, support long-term mitigation strategies, and strengthen the resilience of seismically active mountain road corridors.

### 1.1. Study area

The study is focused on the northwestern region of Kathmandu, the capital city of Nepal, characterized by dissected tropical landscapes with notable geomorphological evidence of historical landslides (Ghimire *et al.*, 2008). This

region is home to two significant landslides that occurred in the mountain villages and along the Pasang Lhamu Highway. Among these, the Ramche landslide, which spans approximately 3 km along the Pasang Lhamu Highway near Ramche village, is the most prominent. The highway is a vital route for transporting goods between Nepal and China, thus subjecting the landslide area to considerable vibrational stress.

The study sites are situated in the Kalika Rural Municipality of the Rasuwa District within Bagmati Province, Central Nepal. Geographically, the area lies between 85°12' 00''E to 85°15' 00''E and 28°00' 00''N to 28°03' 00''N (Fig. 1). The terrain is predominantly mountainous, featuring rugged topography with steep hills and flat river terraces. The Ramche landslide is located at the base of the Trishuli River, while the Dhaibung landslide is

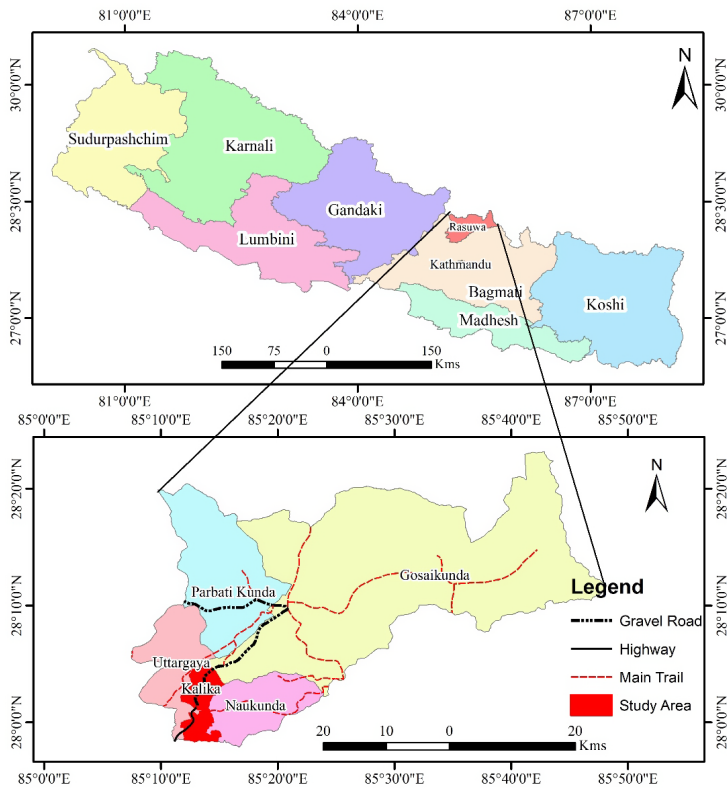


Fig. 1. Location map of the study area. The landslides under observation lie within the area marked by the red colour.



situated along the Phaleku Khola. Both landslides contribute to regional drainage systems, as their runoff flows into the Trishuli River and Phaleku Khola, respectively. Rasuwa District experiences a range of climatic conditions, from the temperate climate in the southern lowlands to a polar tundra climate in the northern highlands. Precipitation is highest during the summer monsoon months of July and August, with an average of 880 mm, while November and December, the winter months, and receive the least precipitation, averaging 20 mm. The heavy monsoon rainfall in the region is largely attributed to moisture-laden air and the orographic effect (*Boos and Kuang, 2010*), while the winter season is marked by dry, cold air and significantly reduced precipitation levels (*Shrestha et al., 2012*).

## 1.2. Regional geological context

The study area lies within the Kuncha Formation of the Lesser Himalayan Metasediments in central Nepal, as identified by *Stöcklin and Bhattarai (1977)*. This formation is equivalent to the Ranimata Formation according to the classification by the Department of Mines and Geology (*DMG, 2011*) (Fig. 2). Geologically, the region belongs to the Lesser Himalayan Sequence,

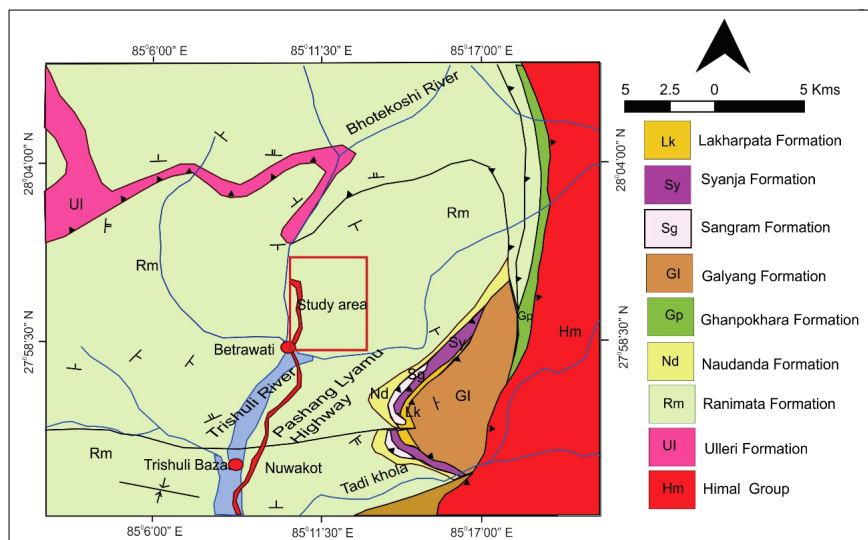


Fig. 2. Generalized geological map of Central Nepal showing the major geologic subdivisions (modified from *DMG, 2011*). The study area is demarcated by a square box.

more specifically the Midland Group, which comprises the Lakharpata and Dailekh Subgroups. These subgroups include several formations such as the Kushma, Seti, Naudanda, and Ghanpokhara Formations, along with the Ulleri Gneiss. The dominant lithologies in the area are quartzite, phyllite, metasandstone, and carbonaceous phyllite, with occasional limestone and dolomite intercalations. In addition, recent unconsolidated deposits such as alluvium and colluvium are also present. A significant geological feature of the region is the Main Central Thrust (MCT), which traverses the area.

The landslide-prone zones are primarily composed of phyllite, schist, and metasandstone of the Ranimata Formation. The Ramche landslide area is oriented towards the northeast (NE) with slope dips ranging from 30° to 40°, whereas the Dhaibung landslide area faces southeast (SE) and exhibits dip angles between 25° and 45°.

## 2. Methodology

This study introduces a comprehensive approach that integrates multiple methods, including field-based geological and geomorphological study, geophysical investigations, geotechnical analysis, and clay mineralogy, to characterize the Ramche and Dhaibung landslides.

### 2.1. Geological and geomorphological study

The field surveys were preceded by analysing Google Earth images for geomorphic analysis, which generated preliminary information on the landslides. The main methodologies adopted in this study were detailed geomorphological analysis, engineering geological mapping for the geological survey.

The geological field survey within and adjacent to the landslide area was conducted by thoroughly examining the rocks for identification and further geological structures (tension cracks, fractures, major joint sets, and other deformation structures) were observed. Additionally, various features and parameters such as attitude and foliation planes, weathering patterns and depth, boulder dimensions, and soil types were documented. The engineering geological maps were prepared for each landslide, which are considered crucial for offering a clearer understanding of the morphology and depicting surface geology.

## 2.2. Geophysical investigation

A Geophysical survey, specifically Electrical Resistivity Tomography (ERT), was conducted using a multifunctional digital DC electrical Resistivity instrument (Geomative, GD-10) accompanied by a multiplex electrode converter (CS60), to analyse the subsurface lithology and identify the slip surface of the landslide. Owing to its adequate sensitivity to both vertical and horizontal changes in subsurface resistivity, as well as its effective depth of penetration for investigation., Wenner array with electrode spacing of 5 m was used for data acquisition, ERT data were collected along four profiles (ERT 1, ERT 2, ERT 3, and ERT 4) each extending 300 metres in length, with a maximum investigation depth of approximately 60 metres for both landslides (Fig. 3). The acquired data were later processed and analysed using RES2D-INV software employing nonlinear optimization technique for 2D inversion analysis (Loke *et al.*, 2013; Khan *et al.*, 2021).

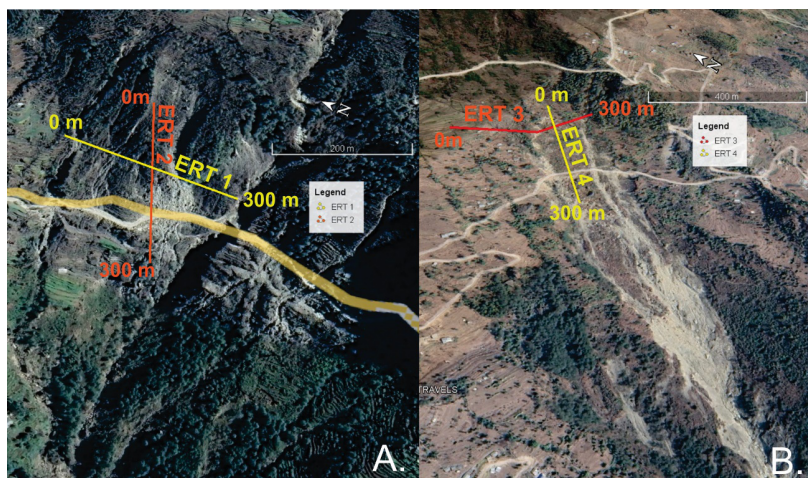


Fig. 3. The landslides are shown on the Google Earth image with locations of different ERT profiles represented as solid lines, A) Ramche landslide and B) Dhaibung landslide.

## 2.3. Soil sampling and geotechnical investigation

A total of 6 representative samples (3 from Ramche and 3 from Dhaibung landslides) were collected from the topsoil at a depth of 50 cm and placed in a plastic bag, and taken to the laboratory to analyse the soil's index

properties. The particle size distribution was conducted using the ASTM standard sieve.

The Liquid Limit, Plastic Limit, and Plasticity Index were determined using standard procedures (ASTM D 4318). The Atterberg limits – including liquid limit, plastic limit, and plasticity index – serve as fundamental indicators of soil plasticity in response to changes in moisture content.

The moisture content of the soil and specific gravity, and unit weight were also determined.

A direct shear test was conducted to determine the friction angle and cohesion of the collected samples.

The clay mineral composition was determined by analysing the clay fraction using X-ray Diffraction (XRD) machine with advanced Bruker D8 diffractometer equipped with a copper (Cu) cathode and a Nickel (Ni) filter under standardizes working conditions. This analysis aimed to understand the weathering patterns influencing the landslide-prone slopes. To assess the role of clay minerals in the Ramche and Dhaibung landslides, representative samples (RM-1, RM-2, RM-3, DB-1, DB-2, and DB-3) were selected for laboratory testing.

The Kubler Index (KI), an indicator of illite crystallinity and diagenetic grade, was determined both manually and using computer software. As reported by *Awan and Kimura (1996)*, the difference between manual and computer-derived KI values is generally negligible.

## 2.4. Slope stability assessment

The slope stability assessment was conducted using the limit equilibrium method (LEM) in Slide software under normal dry and saturated, and upon seismic load under the dry and saturated conditions. Various LEMs are available for slope stability analysis, categorized into rigorous and non-rigorous methods. These include the Ordinary, Bishop, Morgenstern, and Janbu methods, which has been adopted in this study (*Zhao et al., 2015; Wang et al., 2021*). Cohesion, frictional angle, unit weight, ground water table, and slope geometry were used as an input parameters. Horizontal load of 0.3 and vertical load of 0.2 were applied for analysis under seismic load based on (Seismic Design of Buildings in Nepal, *NBC 105, 2020*). The critical factor of safety for the slope under different conditions was determined, which was then used for the inference of the instability of the slope.

### 3. Result

#### 3.1. Geomorphological characteristics

##### *Ramche landslide*

Geomorphologically, the Ramche landslide faces west and is covered with a thick colluvium mass over the rocky terrain. The slope ranges from  $25^\circ$  to  $45^\circ$ , with the vertical elevation difference of  $\sim 1.5$  km from toe to crown. The landslide features three prominent active crowns and numerous gullies, some with flowing water. Serving as a significant drainage system for the region, the landslide terminates as a stream with substantial water discharge into the Trishuli River. The crown of the landslide is located approximately 300 metres above the highway, causing damage to the gabion walls intended to contain the large boulders within the debris.

##### *Dhaibung landslide*

Similarly, the Dhaibung landslide is situated along the Kalikasthan to Jibjibe road section. It covers an area of 0.3 square kilometres and extends over a length of 3 kilometres, with a width varying between 80 to 100 metres. The Dhaibung landslide is situated in the southwest slope direction and is characterized by thick colluvium covering rocky terrain, with an elevation ranging from 715 to 2085 metres and slopes between  $20^\circ$  to  $40^\circ$ . This extensive landslide, moving towards Jibjibe, features a prominent crown section marked by numerous tension cracks, remnants of past debris, and significant accumulations of boulders. Serving as a primary drainage, the landslide directs water flow towards the Phaleku Khola, leading to heightened water discharges, particularly during the monsoon seasons. This increased water flow renders the route impassable during such periods. The relatively stable Dhaibung landslide before the 2015 Gorkha Earthquake has recently been reactivated after the earthquake event.

#### 3.2. Engineering geological study

##### *Ramche landslide*

Engineering geological mapping was carried out to assess the geomaterial and structural characteristics of the Ramche landslide along the Pasang Lyamu or Rasuwa Kerung Highway (Fig. 4). The landslide is subdivided into three major morphological zones: the crown, body, and toe, each dis-

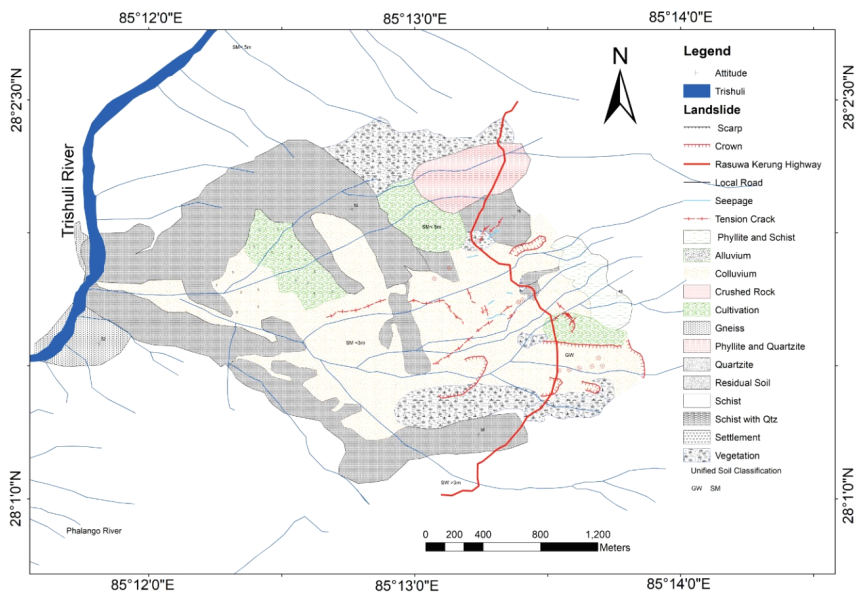


Fig. 4. Detailed engineering geological map of the Ramche landslide and surrounding area.

playing distinct geological and geomorphological conditions.

The crown zone, located in the northern upper slope, predominantly comprises a layer of colluvium ranging from pebbles to large boulders resting over highly weathered, jointed, and fractured bedrock composed mainly of grey to greenish-grey phyllite. The colluvium exhibits high permeability due to its loose matrix of mixed coarse materials and sandy soil (Fig. 5A). The rocks exhibit prominent foliations with variable attitudes, commonly dipping southwest at moderate angles, which in many cases are unfavorably oriented towards slope faces, increasing the likelihood of planar failures. The slope angle in the crown ranges between  $15^{\circ}$  and  $50^{\circ}$ , and several vertical and inclined tension cracks are visible in both the colluvium and underlying bedrock, indicating active deformation. Seasonal drainages and debris-filled gullies are also common, contributing to surface runoff concentration and further destabilisation (Fig. 5B).

In the body of the landslide, a thick, wedge-shaped colluvial deposit is present. This zone contains a heterogeneous mixture of gravels, cobbles, boulders, sands, and minor residual soils. It is intersected by the Rasuwa

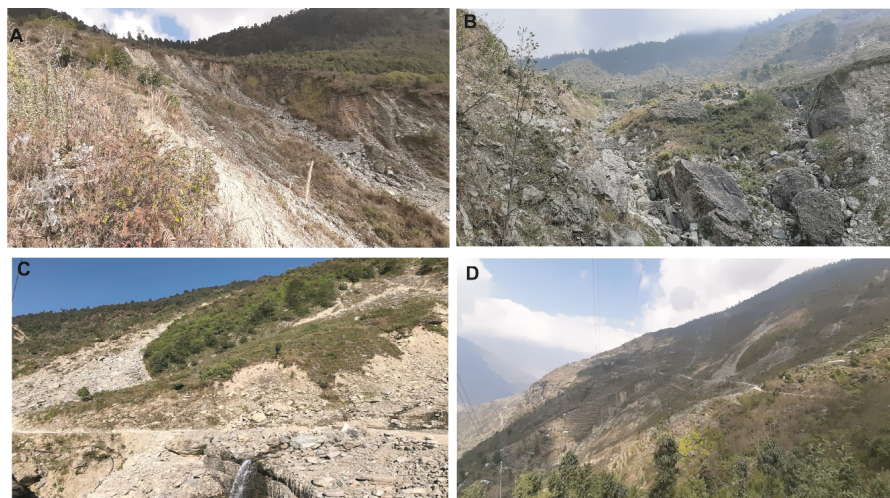


Fig. 5. Field observations showing surface deformation caused by the Ramche landslide – (A) crown area with abundant colluvium deposits, (B) overall view of the Ramche landslide, (C) main body showing an unstable road traversing the landslide zone, and (D) wide view of the toe section.

Kerung Highway, which overlays older abandoned road alignments, both of which exhibit signs of continual downslope movement. Numerous open tension cracks are distributed throughout this zone, especially near infrastructure, indicating ongoing mass displacement. Water is flowing and channelized throughout the body section (Fig. 5C). Lithologically, the area is composed of schist and phyllite, gneiss with foliations and joint sets that dip parallel or sub-parallel to the slope direction, creating structurally unfavorable conditions.

The toe section is situated near the confluence of the Trishuli and is composed of saturated colluvial materials containing cobbles, pebbles, and boulders up to 5 metres in diameter. These deposits are loosely packed and appear to be reworked by both fluvial and mass movement processes. Several gullies were present towards the toe direction (Fig. 5D). Toe erosion by the river contributes to the removal of lateral and basal support, exacerbating the instability of the upper slope mass. Seepage zones and springs identified near lithological contacts and within the colluvium further reduce effective stress and shear strength, facilitating continued displacement.



*Dhaibung landslide*

The Dhaibung landslide, Kalikasthan to Jibjibe road section, exhibits a structurally complex and geologically sensitive terrain extending from the elevated slopes in the north to the riverbanks in the south. The landslide is segmented into three zones: crown, body, and toe, each demonstrating distinct geological features and instability indicators (Fig. 6).

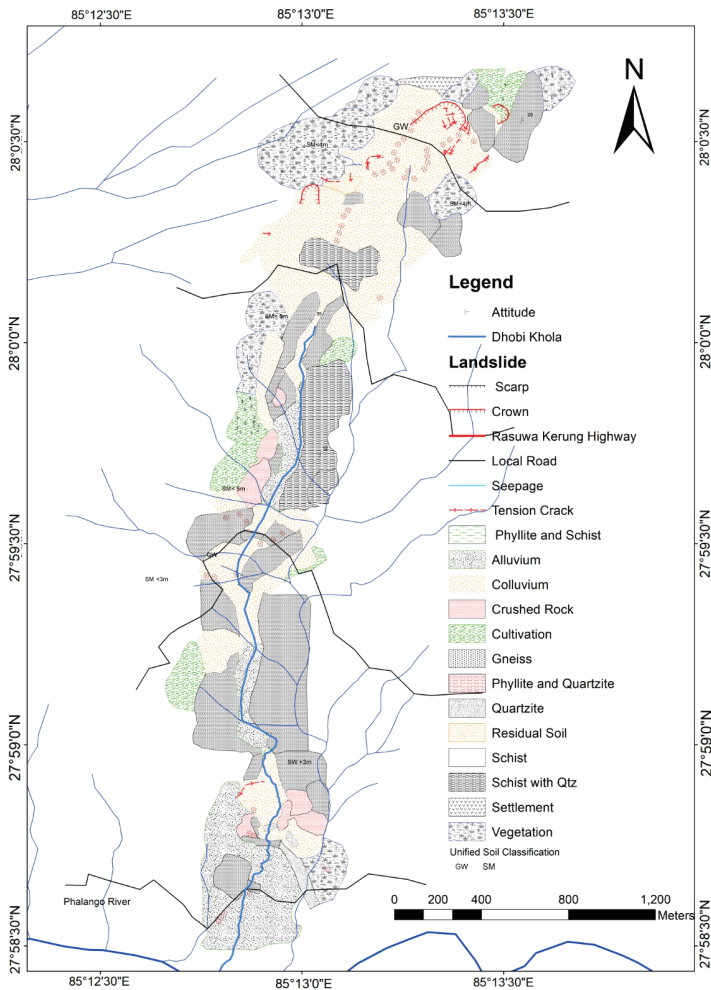


Fig. 6. Detailed engineering geological map of the Dhaibung landslide and surrounding area.



The crown section lies at the upper slope near the head scarp and is primarily composed of residual soil, colluvium, and crushed phyllite and schist, which have undergone significant weathering. The bedrock units here include phyllite, schist, and schist interlayered with quartzite, all of which are heavily fractured and jointed (Fig. 7A). The foliation planes in this zone show southwest dips often daylighting into the slope, thus promoting translational failures. Multiple tension cracks and seasonal seepage lines are observed, particularly along the contact of residual soil and weathered bedrock, which facilitates water infiltration and destabilizes the slope mass.

The body of the landslide extends downslope and consists largely of thick colluvial deposits, estimated at 10–25 m in thickness, composed of a heterogeneous mixture of boulders, cobbles, gravels, and sandy matrix. These materials are weakly consolidated, exhibit high permeability, and are traversed by several seepage zones, indicating high groundwater influence. Interbedded bedrock outcrops of gneiss, quartzite, and phyllite with quartzite, showing differential weathering. Numerous tensional cracks across the body section are aligned with road infrastructure and cultivation zones, implying continued slope movement and deformation, which damages the gabion and other retaining structures (Fig. 7B and Fig. 7C). The Kalikasthan to Jibjibe road cuts across this lower portion of the active landslide, and local

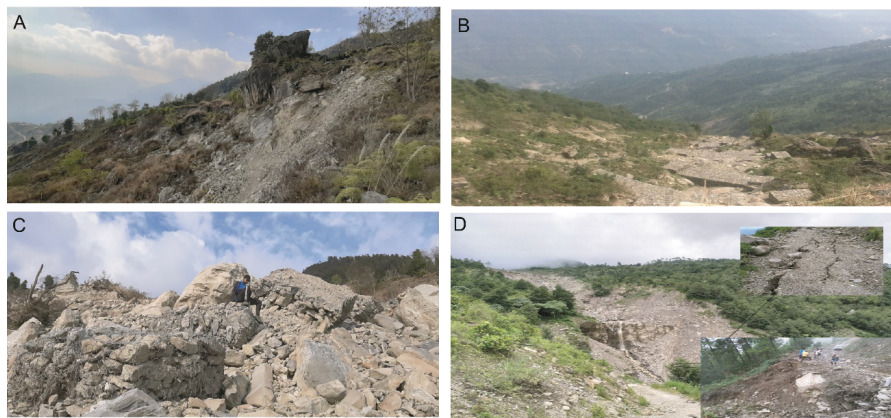


Fig. 7. Field observations showing surface deformation caused by the Dhaibung landslide – (A) deformed rock and abundant colluvium deposits at the crown area, (B) gully management through cascade gabion walls, (C) damaged gabion walls resulting from debris movement, and (D) downslope toward toe displaying road disruption and surface cracks.

access tracks appear reactivated or buried by debris, emphasizing long-term instability (Fig. 7D).

At the toe of the landslide towards downslope, the deposit fans out toward the Dhobhi Khola and Phalango River confluence. This section comprises mainly alluvial and colluvial deposits, including loosely packed cobbles and boulders (some up to 3–5 m in diameter), which are prone to erosion and undercutting by river action (Fig. 6).

### 3.3. Geophysical investigation

The Electrical Resistivity Tomography (ERT) profiles (Fig. 8A and Fig. 8B) of the Ramche landslide area reveal zones with high resistivity values exceeding  $5000\ \Omega\cdot\text{m}$ . The ERT sections of the Ramche landslide reveal distinct subsurface characteristics crucial to understanding slope instability. The uppermost layer consists of dry colluvium, characterized by high resistivity values ranging from over  $1000$  to  $8000\ \Omega\cdot\text{m}$ , extending to a depth of approximately 10 to 15 metres, indicating loose, dry slope materials.

As one moves upslope, the surface clay layer shows an increasing concentration of gravel, mostly ranging from 1 to 2 cm in diameter, although occasionally larger boulders over 1 meter across are encountered. These coarse materials contribute to the elevated resistivity observed at the surface, which extends down to depths of 10 to 15 metres. Towards the southern portion, the thickness of this colluvium increases and reaches up to 40–50 m from the surface.

Beneath this lies the slip surface, identified at depths of about 15 metres, with intermediate resistivity values around  $450$  to  $1000\ \Omega\cdot\text{m}$ , marking the shear interface responsible for movement. The variation in electrical properties among the geological layers enables the ERT profile to delineate the sliding surface's morphology (Sigdel and Adhikari, 2020b). Below the slip surface, a saturated zone is evident, with low resistivity values typically ranging from  $133$  to  $450\ \Omega\cdot\text{m}$ , indicating water-saturated colluvium and fractured bedrock. This saturated zone begins around 10 to 15 metres depth and extends deeper, with fractured and saturated bedrock dominating the lower sections. These low-resistivity zones are critical in controlling landslide dynamics, as the high-water content within the fractured bedrock significantly reduces material strength. Additional features such as cracks and fractures are seen throughout the profiles, especially near the mid to lower slopes,

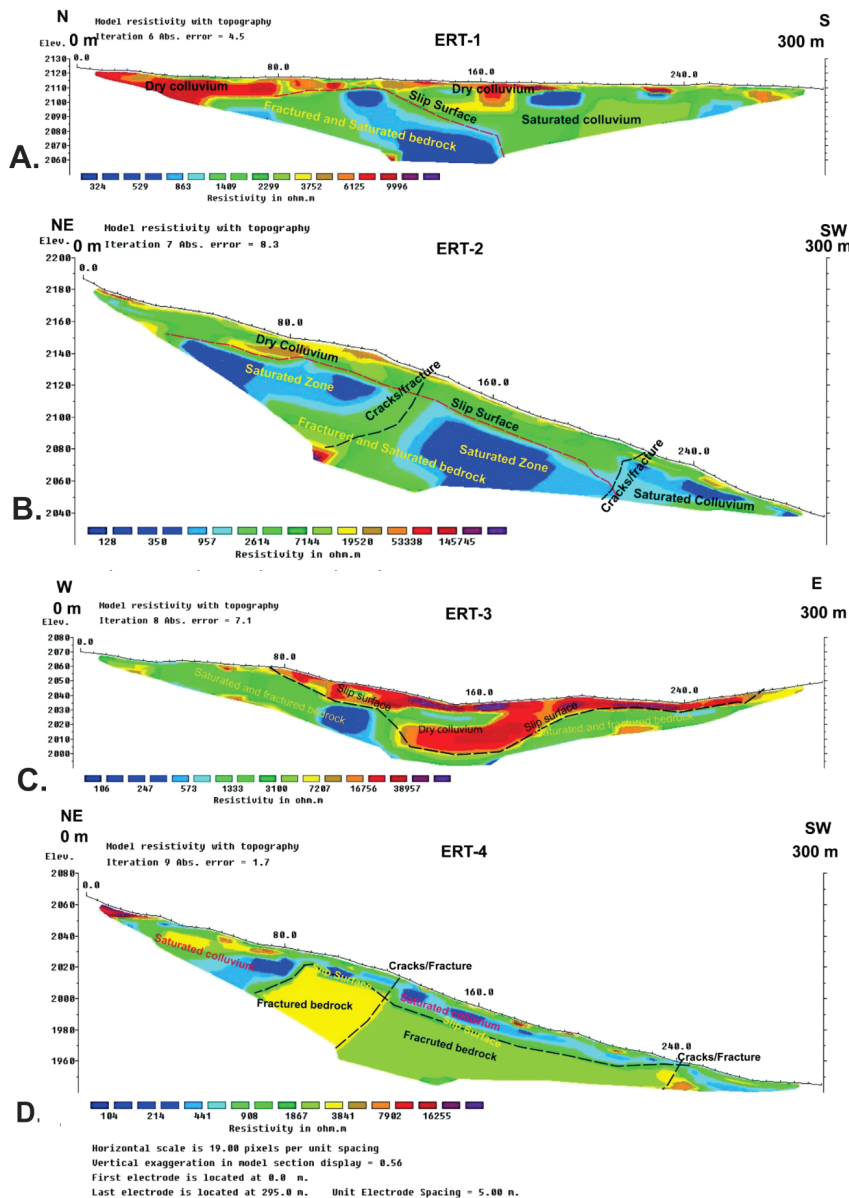


Fig. 8. 2D inversion model from the Electrical Resistivity Tomography of A) Ramche landslide along ERT 1; B) Ramche landslide along ERT 2, C) Dhaibung landslide along ERT 3, and D) Dhaibung landslide along ERT 4.

and the water table is consistently aligned with the low-resistivity zones.

Additionally, the ERT data suggest that the slip surface serves as the boundary of the colluvial aquifer, indicating full saturation of the materials in this zone at 15 m. The groundwater table is located below a depth of 10–15 metres. Similarly, based on the resistivity values observed in the field along the electrical profile, the slope materials of the landslide are classified into four main layers: the colluvium layer, the highly saturated zone, and the highly fractured rock layer.

The Electrical Resistivity Tomography (ERT) profiles of the Dhaibung landslide area provide detailed subsurface imaging that highlights the internal structure of the landslide mass and its controlling factors. The profile (Fig. 8C), taken across the body of the landslide (W–E direction), reveals a surface layer of colluvium with relatively high resistivity values (above  $1000\ \Omega\cdot\text{m}$ ), suggesting dry or moderately moist, loose slope materials. This layer is observed extending to depths of approximately 5 to 10 metres. At the central body part, the colluvial layer lies in the deepest area and reaches up to 35 m from the surface. Beneath this, resistivity decreases sharply in certain zones, corresponding to saturated and fractured bedrock, where values drop to below  $200\text{--}2000\ \Omega\cdot\text{m}$ . These low-resistivity regions occur more prominently in the middle and lower parts of the section and indicate zones of high moisture content, possibly marking the phreatic surface or water-saturated materials that play a critical role in weakening the slope. The contrast resistivity at depths 15–20 m resembles the slip surface of this landslide.

In the second profile (Fig. 8D), taken longitudinally along the landslide from crown to toe (NE–SW direction), the internal layering is even more clearly defined. Near the crown, a zone of saturated colluvium with cracks is identified, characterized by low to moderate resistivity values ranging from 80 to  $600\ \Omega\cdot\text{m}$ . This transitions downslope into a well-defined slip surface, visible as a continuous, relatively narrow band of intermediate resistivity ( $\sim 450\text{--}1000\ \Omega\cdot\text{m}$ ), separating the overlying colluvial deposits from the underlying fractured bedrock. The slip surface varies in depth along the slope, typically occurring around 10 to 15 metres from the surface, and dips gradually toward the toe. Beneath this interface, the fractured and saturated bedrock zone dominates, with resistivity values dropping below  $200\ \Omega\cdot\text{m}$ , indicating significant groundwater presence.

3.4. Geotechnical characterization

The grain size distribution of the soil profile shows predominantly coarse fractions. The grain distribution curves presented in Fig. 9 show strong analogies in their grain size composition with an inadequate fine-grained fraction of approximately 5%. The results indicate that the Ramche landslide comprises approximately 25–30% gravel, 35–40% coarse sand, 10–15% medium sand, 5–15% fine sand, and 4–5% fine silt and soil. The low presence of fine particles suggests either unfavorable conditions for their formation or their entrainment by runoff into streams (*Komadja et al., 2021*). Similarly, grain size distribution of Dhaibung landslide suggests that the soil ranges from 35–40% gravel, 25–30% coarse sand, 10–15% medium sand, 12–15% fine sand and 4–5% silt or soil (Fig. 9). The distribution of grain sizes affects the engineering characteristics of soil and is crucial in determining the frequency and speed of landslides (*Yalcin, 2011*). According to the Unified Soil Classification System (USCS), the landslide soil was classified as well-graded sands, gravelly sands, with little fines, suggesting that no significant influence of particle size distribution on the mechanical behaviour of the slope materials.

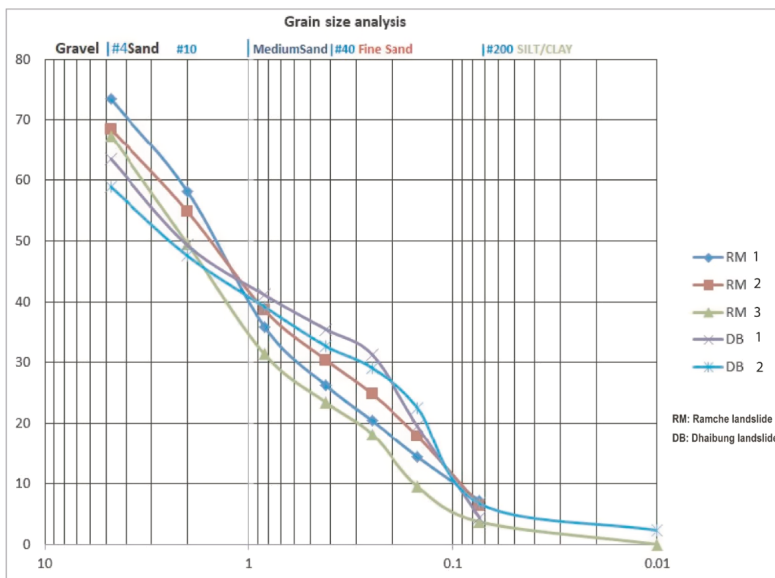


Fig. 9. Grain size distribution of soil samples.

Atterberg limits, including liquid limit and plasticity index, were utilized to classify the fine-grained fraction of soils, as detailed in Table 1. For the Ramche landslide, the liquid limits of the slope soils selected for this study range from 34.54% to 41.78%, while for the Dhaibung landslide, they range from 27.22% to 48.85%. According to Casagrande’s classification (Casagrande, 1948), soils with a liquid limit exceeding 50% are categorized as highly plastic, those with a liquid limit between 30% and 50% exhibit intermediate plasticity and compressibility, and soils with a liquid limit below 30% demonstrate low plasticity. The plasticity index ranges from 6–10% for Ramche landslide and 6–19% for Dhaibung landslide. Based on Casagrande’s classification, the liquid limit of the selected slope soils falls under the category of intermediate plasticity and compressibility for the Ramche landslide and ranges from low to intermediate plasticity for the Dhaibung landslide.

Table 1. Geotechnical laboratory experimentation results (moisture content, Atterberg limits, specific gravity and density, and shear strength parameters) of the soil samples.

		Ramche landslide			Dhaibung landslide		
samples		RM1	RM2	RM3	DB1	DB2	DB3
moisture content (W%)		29.29	31.11	27.78	20.88	35.19	27.78
strength parameter	cohesion (c) Kpa	0.59	0.52	0.65	0.8	1.01	0.68
	angle of friction ( $\phi^\circ$ )	27	28	31	26	29	28
liquid limit (LL)		37.97	41.78	34.54	47.33	48.85	27.22
plastic limit (PL)		29.29	31.11	27.78	27.78	35.19	20.88
plasticity index (PI)		8.69	10.66	6.76	19.52	13.66	6.34
specific gravity (Gs)		2.33	2.4	2.415	2.396	2.172	2.1
dry density (g/cm <sup>3</sup> )		1.185	1.2	1.038	1.011	1.016	1.1
bulk density (g/cm <sup>3</sup> )		1.31	1.348	1.2506	1.06	1.099	1.08

Similarly, the specific gravity for Ramche landslide ranges from 2.3 to 2.4, dry density ranges from 1.0 to 1.2, and bulk density ranges from 1.2 to 1.3, whereas 2.1–2.3, 1.0–1.1, and 1.06–1.09 for Dhaibung landslide, respectively. The direct shear test results of all samples were expressed in terms of the linear Mohr-Colomb failure criterion. The calculated friction angle and cohesion ranges from 27°–31°and 0.52–0.65 for the Ramche landslide and 26°–28°and 0.68–1.01 kPa for the Dhaibung landslide.

### 3.5. Weathering and mineral composition

The XRD analysis revealed that the primary mineral present is quartz, with minor components including plagioclase and calcite. The grain size distribution of the slope materials indicates a minimal presence of silt and clay-sized particles, suggesting a low degree of weathering in the landslide materials (Fig. 10). This aligns with the XRD findings, which highlight the predominance of quartz and the lack of significant expandable clay minerals that could contribute to slope instability under undisturbed conditions (Komadjja *et al.*, 2021).

The active erosion of the landslide mass, observed through the geomorphological evaluation of past satellite images, suggests that chemical weath-

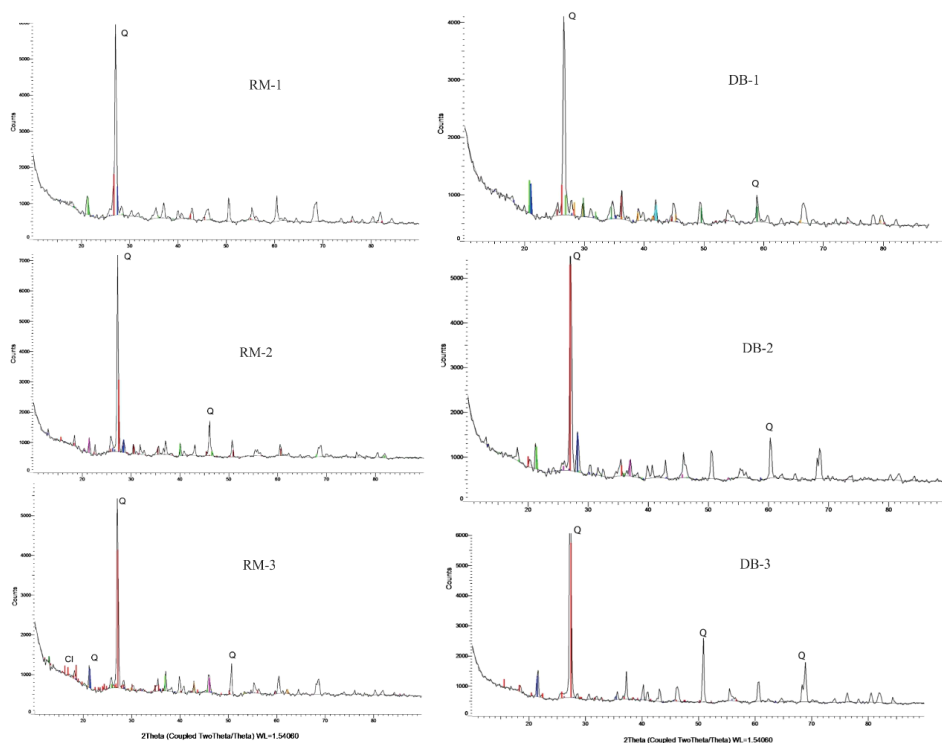


Fig. 10. X-ray Diffraction (XRD) patterns of clay fraction samples from the Ramche (RM-1, RM-2, and RM-3) and Dhaibung landslides (DB-1, DB-2, and DB-3), indicating the presence of dominant minerals.

ering is not taking place, with erosion being most prominent during the rainy season. Consequently, the lack of clay minerals indicates that the slope material failure in both landslides is not due to rock weathering but is instead dependent on rainfall (*Summa et al., 2010*). Non-swelling detrital minerals like quartz interact with water, potentially causing complete slope collapse under heavy or prolonged rainfall. This interaction could explain debris movement in slope areas compared to other debris slides triggered by swelling clay minerals (*Liu et al., 2017*).

### 3.6. Slope stability analysis

According to the results of laboratory experiments, the site investigation, geophysical surveys, as well as engineering geological characteristics, the parameters used for slope stability analysis were comprehensively analysed for both Ramche and Dhaibung landslides. Stability analyses were conducted across four profiles using the Limit Equilibrium Method: in dry conditions, drained conditions, seismic loading in dry conditions, and seismic loading with drained conditions. The Slide software required various input parameters for stability analysis, including cohesion, frictional angle, unit weight, groundwater table, and landslide cross-section data. Seismic analyses involved applying horizontal and vertical loads of 0.3 and 0.2, respectively, as per the Seismic Design of Buildings in Nepal (*NBC 105, 2020*).

The Ramche and Dhaibung landslides consist of two major lithology types: the upper layer consists of a mixture of sediments (sand, clay, gravel, pebbles, and boulders), while the base consists of fractured bedrock, including phyllite and metasandstone. In between these materials slip surface is considered based on ERT interpretation. The depth of the slip surface is used to calculate the factor of safety (FoS) for both landslides.

The stability analysis for both dry and saturated conditions yield factor of safety values of 1.402, 1.436, 1.434, and 1.394, and 0.909, 0.917, 0.921 and 0.908 for the Ordinary, Bishop, Morgenstern, and Janbu methods, respectively (Fig. 11). However, under seismic loading, the factor of safety decreases 0.869, 0.905, 0.908 and 0.908 for dry conditions, and further decreases to 0.575, 0.587, 0.591, and 0.57 for drained conditions (Table 2). These findings suggest that the Ramche landslide is stable under dry conditions but unstable under drained conditions and seismic loading. Due to an increase in pore water pressure, the shear strength decreases, and hence



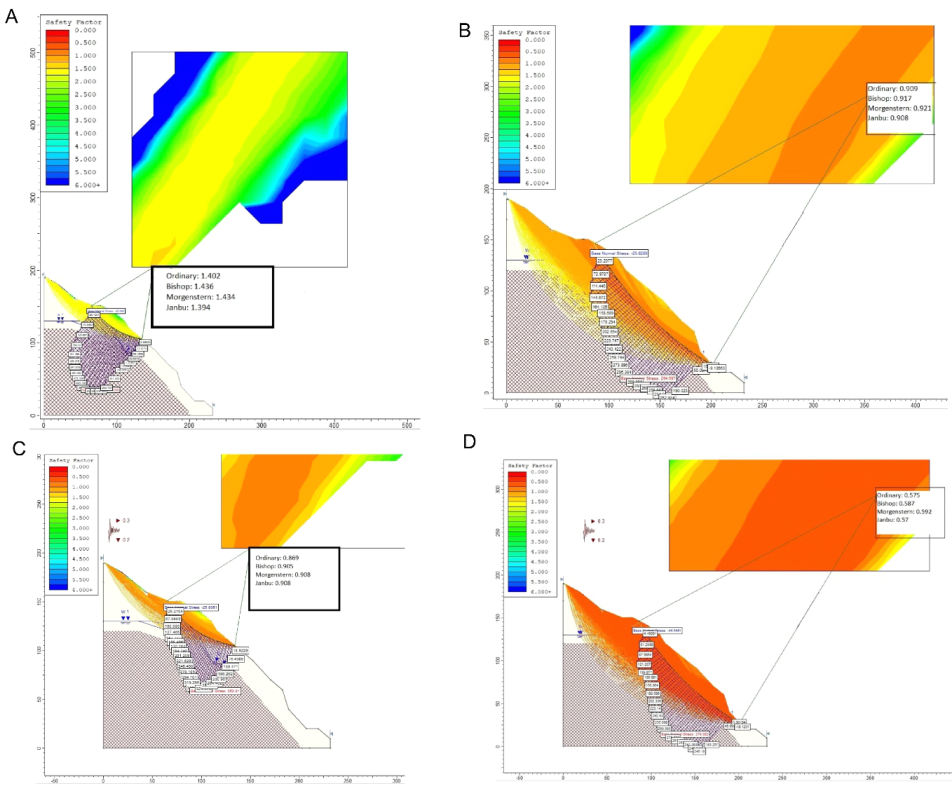


Fig. 11. Slope stability analysis of the Ramche landslide area using the Limit Equilibrium Method in SLIDE software – (A) present slope condition showing stability with Factor of Safety (FoS) values above 1.4, (B) slope condition after rainfall infiltration, showing reduced FoS (0.91–0.93), (C) condition under Seismic loading, with FoS further decreasing to approximately 0.86, and (D) critically unstable scenario with significantly reduced FoS (0.57–0.59) in saturated condition and seismic loading, indicating potential slope failure. The analysis uses multiple methods, including Ordinary, Bishop, Morgenstern-Price, and Janbu, with FoS distribution illustrated through colour contours.

the FoS of the slip surface is reduced, which enhances slope failure for the undrained condition.

Similarly, the stability analysis for the Dhaibung landslide indicates factor of safety values of 1.283, 1.238, 1.237, and 1.165 under dry conditions, and 1.408, 1.375, 1.376, and 1.297 under saturated conditions for various Limit Equilibrium Methods (LEMs). However, when subjected to seismic

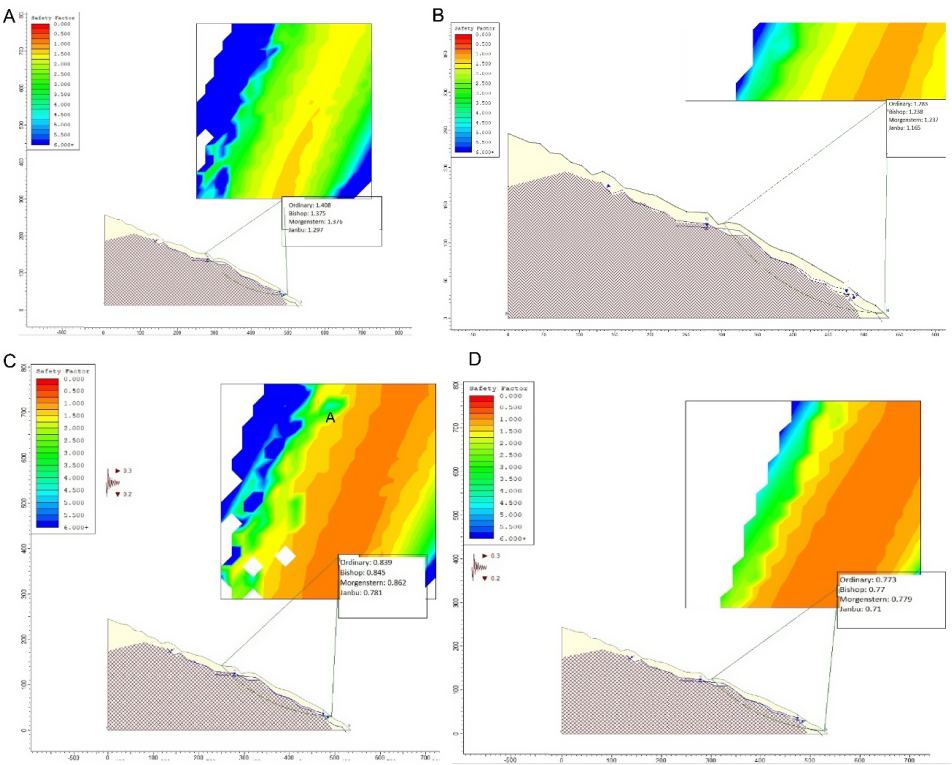


Fig. 12. Slope stability analysis of the studied landslide site using four different limit equilibrium methods (Ordinary, Bishop, Morgenstern-Price, and Janbu). (A) Stability under dry conditions showing a factor of safety above 1.0, indicating slope stability, (B) stability under partially saturated conditions with slightly reduced safety factors but still stable, (C) stability under fully saturated conditions with safety factors below 1.0, indicating potential slope failure, and (D) stability under saturated conditions combined with seismic loading, showing further reduced safety factors and higher landslide risk. Colour contours represent the factor of safety values: orange indicates failure zones (FoS <1), while green to blue represents stable zones (FoS >1).

loading, the factor of safety decreases to 0.773, 0.77, 0.779, and 0.71 under dry conditions, and to 0.839, 0.845, 0.862, and 0.781 under saturated conditions for all LEM methods used in the analysis (Fig. 12; Table 2) These results indicate that the slope remains marginally stable under both dry and saturated conditions, but becomes unstable when subjected to external forces such as seismic loading.

Table 2. Factor of safety (FoS) values for Ramche and Dhaibung landslides under various slope conditions using the limit equilibrium method (LEM).

slope	conditions	FoS (LEM)			
		OMS	BSM	MPM	JB
Ramche landslide	dry	1.402	1.436	1.434	1.394
	saturated	0.909	0.917	0.921	0.908
	seismic load (dry)	0.869	0.905	0.908	0.85
	seismic load (saturated)	0.575	0.587	0.592	0.57
Dhaibung landslide	dry	1.283	1.238	1.237	1.165
	saturated	1.408	1.375	1.376	1.297
	seismic load (dry)	0.773	0.77	0.779	0.71
	seismic load (saturated)	0.839	0.845	0.862	0.781

4. Discussion

The formation mechanisms of the Ramche and Dhaibung landslides are governed by a complex interaction of geological, geomorphological, geotechnical, mineralogical, hydrological, and anthropogenic factors, all of which collectively contribute to slope instability in the region. Despite their occurrence within a similar lithological and topographic setting, these landslides exhibit variations in failure behaviour that reflect localized differences in subsurface conditions, surface processes, and external triggers.

The evidence of geomorphic analysis by Google Earth image illustrate lateral expansion of landslide boundaries, road displacements, and shifting of residential infrastructure well correlates with active erosion, development of tension cracks, and the formationof debris channels, prominently in the Dhaibung landslide area, indicating long-term instability processes. Erosional gullies, more abundant at Dhaibung, enhance surface runoff and sediment transport, generating debris-rich colluvial layers that dominate the landslide mass and influence material behaviour during heavy rainfall events.

The subsurface configuration revealed through Electrical Resistivity Tomography (ERT) strongly supports surface observations and geotechnical findings by identifying critical internal features that govern landslide be-

haviour. ERT profiles across both Ramche and Dhaibung landslides display distinct low-resistivity zones associated with water-saturated zone and fractured rocks, as well as high-resistivity zones indicative of coarse, dry colluvium. These contrasting resistivity patterns delineate weak, unconsolidated deposits, fractured zones, and potential slip surfaces distributed at varying depths within the landslide mass (*Jongmans and Garamboish, 2007; Asriza et al., 2017; Sigdel and Adhikari, 2020b*). The identification of electrically conductive zone extending through the slope body highlights the presence of preferential infiltration pathways and perched groundwater tables, which contribute to elevated pore pressure during intense monsoonal rainfall. This infiltration process is further complicated by the permeability contrast between the gravel-rich colluvial cover and the underlying weathered bedrock. The upper colluvium, comprising approximately 20–25% gravels, facilitates rapid percolation of surface water. However, the lower permeability of the underlying phyllite and metasandstone bedrock promotes the accumulation of groundwater at the contact zone. This accumulation results in progressive saturation and softening of the weathered bedrock interface, which serves as a shear zone and potential slip surface. The presence of these weak zones and their hydrological connectivity is indicated in the ERT sections and is corroborated by geotechnical tests that show decreased shear strength under natural saturated conditions. Slope stability analysis reflects this behaviour, with the Factor of Safety dropping below unity under both dry and saturated scenarios, indicating a critical state of instability.

Further geotechnical evaluation, including Atterberg limit testing, classifies the soil as having low to intermediate plasticity and compressibility, characteristics that amplify susceptibility to failure under heavy and prolonged rainfall events (*Rathore et al., 2024*). Continuous infiltration not only affects the overlying colluvial materials but also gradually alters the physical integrity of the underlying bedrock. The softening of phyllite and metasandstone in these landslides through sustained water exposure promotes the development of subsurface fractures and tension cracks, particularly along the crown and middle parts of the landslides. These cracks, extending to significant depths—as confirmed by ERT imaging act as secondary infiltration routes, intensifying water retention and pore pressure within the slope mass. The resulting hydrostatic buildup along these fracture planes further weakens structural cohesion, leading to downward displacement of

the entire slope body (*Dahal and Hasegawa, 2008*). This progression from infiltration to deep-seated cracking and eventual displacement defines the dominant failure mechanism observed in both the Ramche and Dhaibung landslides (*Epada et al., 2012*).

The stability of the Ramche and Dhaibung areas was significantly impacted by the 2015 Gorkha earthquake (*Collins and Jibson, 2015; Williams et al., 2018*). During seismic activity, the safety factors for the Ramche and Dhaibung landslides ranged from 0.9 to 0.5 and 0.7 to 0.8 under dry and wet conditions, respectively. This indicates a high risk of surface failure and landslide triggering. These results suggest that earthquakes occurring during the dry season may initiate landslides to some extent, while those during the wet season could worsen movement, ultimately leading to slope failure. These FoS values are broadly consistent with other Nepalese case studies that document large reductions of slope stability during coseismic and saturated states. Post-earthquake investigations following the 2015 Gorkha event and subsequent field/numerical work in Nepal have repeatedly shown that dynamic loading combined with elevated groundwater or rapid infiltration can reduce FoS to values well below unity, particularly for road-cut and fissured slopes (*Roback et al., 2018*). Rainfall-driven saturation alone has also been shown to reduce FoS by 20–40% or more in comparable Himalayan slopes, converting marginally stable slopes (FoS  $\approx$  1.2–1.4) to failure-prone conditions (*Guo et al., 2022; Kamal et al., 2023*).

The geotechnical and mineralogical analyses of the Ramche and Dhaibung landslides reveal a minimal presence of clay minerals, with quartz being the dominant constituent and a notable absence of expansive clay minerals such as smectite, illite, or montmorillonite (*Komadja et al., 2021*). In contrast to clay-rich slopes, where expansive clays like smectite and montmorillonite undergo volumetric changes upon wetting, leading to reduced cohesion, increased pore pressure, and heightened landslide susceptibility (*Huang et al., 2011*), the slope materials in the study area composed primarily of weathered phyllite and metasandstone do not exhibit such behaviours. This indicates that the landslide mechanisms in Ramche and Dhaibung are not governed by clay-induced swelling or shrinkage but are instead driven by hydrological influences, particularly rainfall-induced infiltration into the colluvial cover and underlying weak bedrock (*Summa et al., 2010*). This is further supported by the understanding that in clay-deficient slopes, insta-

bility is primarily caused by reduced effective stress due to increased pore water pressure, rather than material softening or progressive failure from repeated wetting-drying cycles typical in clay-rich environments (*Crosta and di Prisco, 1999; Zhang et al., 2017*).

The structure and fragile geology, and surface geomorphic characteristics along the slope also played a role in triggering the landslide. The abundant gullies, which can enhance surface erosion, can lead to more debris movement during the rainy season. This aligns with the case of the Dhaibung landslide, where more debris-dominant sediments are found in the colluvial cover. This is consistent with FoS remaining more than 1 even when we applied the dry and saturated. Weak geological materials, including weathered phyllite and highly jointed metasandstone, negatively impacted material stability due to their geotechnical and mineralogical characteristics. The combination of these jointed masses, weak lithology, and a slope angle exceeding 35–40 degrees resulted in the dislocation of slope material, leading to the landslide (*Khan et al., 2021*).

Anthropogenic activities further exacerbate slope instability, particularly in the Ramche area, where a major roadway traverses the landslide zone. The continuous movement of heavy vehicles introduces cyclic vibrations that disturb the already loose and saturated soil matrix, accelerating material disaggregation and contributing to slope weakening. This phenomenon is most evident near the road cuts and margins of the Ramche landslide, where displacement patterns and ground settlement are associated with traffic-induced stress (*Komadja et al., 2021*).

Despite these shared instability drivers, the two landslides differ in their mechanical response and overall behaviour. Ramche demonstrates more intense surface deformation, frequent tension cracking, and higher displacement rates, partly due to the lack of competent bedrock at its toe, which allows for unimpeded downslope movement. In contrast, the Dhaibung landslide benefits from the presence of a substantial bedrock mass at its base, which acts as a buttress and enhances its stability. While Ramche is primarily pore-pressure driven, Dhaibung's instability is more closely linked to surface erosion and debris accumulation, illustrating how localized variations in geology and geomorphology modulate landslide mechanisms within similar settings.

## 5. Conclusion

This study provides a comprehensive assessment of the Ramche and Dhaibung landslides located in the Lesser Himalaya of central Nepal, utilizing a multidisciplinary approach that integrates geomorphological observations, geophysical (ERT) imaging, geotechnical testing, and mineralogical analysis. Although both landslides occur within the same regional geological setting, they differ in lithological composition—Ramche is mainly comprised of phyllite, metasandstone, schist, and gneiss, while Dhaibung consists primarily of schist, phyllite, and metasandstone. ERT surveys reveal a transitional slip zone at depths of approximately 10–15 m in Ramche and 15–20 m in Dhaibung, where saturated, low-resistivity layers occur between the loose colluvial cover and underlying weathered bedrock. These zones correspond well with observed surface features such as tension cracks and signs of active movement. Geotechnical characterization shows that both landslides are underlain by loose, non-cohesive colluvial soils with low plasticity, cohesion values between 0.5 and 1.1 kPa, and friction angles ranging from  $27^\circ$  to  $35^\circ$ , indicating poor shear strength under saturated conditions. X-ray diffraction (XRD) results confirm quartz as the dominant mineral phase with minimal clay presence, suggesting mechanical rather than chemical weathering is the key weakening process. Stability analyses reveal that both slopes remain stable in dry conditions ( $\text{FoS} > 1$ ). However, under saturation and seismic loading, the Ramche landslide becomes critically unstable ( $\text{FoS} < 1$ ), whereas the Dhaibung landslide remains marginally stable ( $\text{FoS} > 1$ ), even in saturated conditions. This suggests that in Ramche, pore water pressure buildup due to prolonged rainfall significantly reduces slope stability, while in Dhaibung, surface erosion and gully development are more prominent mechanisms contributing to slope degradation. Comparative imagery and field observations show that Ramche has undergone multiple phases of movement and exhibits more severe deformation features, such as displaced roads and reactivated scars, indicating greater instability than Dhaibung. These findings underscore the key influence of hydrological processes, lithological variability, and structural conditions in landslide development. Collectively, the integrated dataset provides valuable insights into slope failure dynamics and highlights the necessity for targeted mitigation strategies in similar high-risk Himalayan terrain.

**Acknowledgements.** The authors would like to thank Department of Mines and Geology (DMG), Nepal and Nepal Academy of Science and Technology (NAST), Kathmandu for the laboratory support.

## References

- Asriza R. O., Rohadi S., Kristyanto T. H. W., Indra T. L., Syahputra R., Tempessy A. S., 2017: Determination of the Landslide Slip Surface Using Electrical Resistivity Tomography (ERT) Technique. In: Mikos M., Tiwari B., Yin Y., Sassa K. (Eds.): *Advancing Culture of Living with Landslides*. WLF 2017. Springer, Cham, pp. 54–61, doi: 10.1007/978-3-319-53498-5\_7.
- Awan M. A., Kimura K., 1996: Thermal structure and uplift of the Cretaceous Shimanto Belt, Kii Peninsula, Southwest Japan: An illite crystallinity and illite  $b_0$  lattice spacing study. *Isl. Arc*, **5**, 1, 69–88, doi: 10.1111/j.1440-1738.1996.tb00013.x.
- Bhandari B. P., Dhakal S., 2018: Lithological control on landslide in the Babai Khola Watershed, Siwaliks Zone of Nepal. *Am. J. Earth Sci.*, **5**, 3, 54–64.
- Boos W. R., Kuang Z., 2010: Dominant control of the South Asian monsoon by orographic insulation versus plateau heating. *Nature*, **463**, 7278, 218–222, doi: 10.1038/nature08707.
- Borrelli L., Ciurleo M., Gullà G., 2018: Shallow landslide susceptibility assessment in granitic rocks using GIS-based statistical methods. *Landslides*, **15**, 6, 1127–1142, doi: 10.1007/s10346-018-0947-7.
- Casagrande A., 1948: Classification and identification of soils. *Trans. Am. Soc. Civil Eng.*, **113**, 1, 901–930, doi: 10.1061/TACEAT.0006109.
- Chigira M., Yagi H., 2006: Geological and geomorphological characteristics of landslides triggered by the 2004 Mid Niigata Prefecture earthquake in Japan. *Eng. Geol.*, **82**, 4, 202–221, doi: 10.1016/j.enggeo.2005.10.006.
- Collins B. D., Jibson R. W., 2015: Assessment of existing and potential landslide hazards resulting from the April 25, 2015 Gorkha, Nepal earthquake sequence. U.S. Geological Survey, Open-File Report, 1142 p., doi: 10.3133/ofr20151142.
- Crosta G., di Prisco C., 1999: On slope instability induced by seepage erosion. *Can. Geotech. J.*, **36**, 6, 1056–1073, doi: 10.1139/t99-062.
- Cui Y., Yang W., Xu C., Wu S., 2023: Distribution of ancient landslides and landslide hazard assessment in the Western Himalayan Syntaxis area. *Front. Earth Sci.*, **11**, 1135018, doi: 10.3389/feart.2023.1135018.
- Dahal R. K., 2015: Understanding of Landslide Science in the Nepal Himalaya. In: Lollino G., Giordan D., Crosta G. B., Corominas J., Azzam R., Wasowski J., Sciarra N. (Eds.): *Engineering Geology for Society and Territory – 2*. Springer, Cham, pp. 1299–1303, doi: 10.1007/978-3-319-09057-3\_228.
- Dahal R. K., Hasegawa S., 2008: Representative rainfall thresholds for landslides in the Nepal Himalaya. *Geomorphology*, **100**, 3-4, 429–443, doi: 10.1016/j.geomorph.2008.01.014.
- Dangol V., 2006: Status of Landslide Hazard Mapping in Nepal. In: Marui H., Mikoš M. (Eds.): *Disaster Mitigation of Debris Flows, Slope Failures and Landslides*.



- Proceedings of the INTERPRAEVENT international symposium: september 25–29, 2006 in Niigata, Japan, Universal Academy Press, Tokyo, pp. 815–819.
- Delmonaco G., Falconi L., Leoni G., Margottini C., Puglisi C., Spizzichino D., 2005: Multi-Temporal and Quantitative Geomorphological Analysis on the Large Landslide of Craco Village (M118). In: Sassa K., Fukuoka H., Wang F., Wang G. (Eds.): *Landslides: Risk Analysis and Sustainable Disaster Management*. Springer, Berlin, Heidelberg, pp. 113–118, doi: 10.1007/3-540-28680-2\_13.
- DMG, 2011: *Geological Map of Central Nepal*.: Department of Mines and Geology, Kathmandu.
- Epada P. D., Sylvestre G., Tabod T. C., 2012: Geophysical and Geotechnical Investigations of a Landslide in Kekem Area, Western Cameroon. *Int. J. Geosci.*, **3**, 4, 780–789, doi: 10.4236/ijg.2012.34079.
- Galay V., 1987: Erosion and sedimentation in the Nepal Himalaya. An assessment of river processes. Ministry of water resources HMG Nepal, Report no. 4/3/012587/1/1, seq. 259.
- Gerrard J., 1994: The landslide hazard in the Himalayas: Geological control and human action. *Geomorphology*, **10**, 1–4, 221–230, doi: 10.1016/0169-555x(94)90018-3.
- Ghimire T., Paudel L. P., Pant B., 2008: The Devastating Ramche Landslide (Rasuwa) and the Future of Polchet Residents. *J. Nepal Geol. Soc.*, **36**, 27, <https://www.nepjol.info/index.php/JNGS/article/view/787>.
- Guo B., Pei X., Xu M., Li T., 2022: Analyzing rainfall threshold for shallow landslides using physically based modeling in Rasuwa District, Nepal. *Water*, **14**, 24, 4074, doi: 10.3390/w14244074.
- Hasegawa S., Dahal R. K., Yamanaka M., Bhandary N. P., Yatabe R., Inagaki H., 2009: Causes of large-scale landslides in the Lesser Himalaya of central Nepal. *Environ. Geol.*, **57**, 6, 1423–1434, doi: 10.1007/s00254-008-1420-z.
- Huang R. Q., Xu Q., Huo J., 2011: Mechanism and geo-mechanics models of landslides triggered by 5.12 Wenchuan earthquake. *J. Mt. Sci.*, **8**, 2, 200–210, doi: 10.1007/s11629-011-2104-9.
- Jin B., Zeng T., Yin K., Gui L., Guo Z., Wang T., 2024: Dynamic landslide susceptibility mapping based on the PS-InSAR deformation intensity. *Environ. Sci. Pollut. Res.*, **31**, 4, 7872–7888, doi: 10.1007/s11356-023-31688-x.
- Jongmans D., Garambois S., 2007: Geophysical investigation of landslides: A review. *Bull. Soc. Géol. Fr.*, **178**, 2, 101–112, doi: 10.2113/gssgfbull.178.2.101.
- Kamal A. S. M. M., Hossain F., Ahmed B., Rahman M. Z., Sammonds P., 2023: Assessing the effectiveness of landslide slope stability by analysing structural mitigation measures and community risk perception. *Nat. Hazards*, **117**, 3, 2393–2418, doi: 10.1007/s11069-023-05947-6.
- K.C. J., Gautam D., Neupane P., Paudyal K. R., 2018: Landslide inventory mapping and assessment along the Ramche-Jharlang area in Dhading, Rasuwa and Nuwakot districts, Lesser Himalaya Central Nepal. *J. Nepal Geol. Soc.*, **55**, 1, 103–108, doi: 10.3126/jngs.v55i1.22798.
- Keefer D. K., 2002: Investigating landslides caused by earthquakes – A historical review. *Surv. Geophys.*, **23**, 6, 473–510, doi: 10.1023/A:1021274710840.

- Khan M. A., Basharat M., Riaz M. T., Sarfraz Y., Farooq M., Khan A. Y., Pham Q. B., Ahmed K. S., Shahzad A., 2021: An integrated geotechnical and geophysical investigation of a catastrophic landslide in the Northeast Himalayas of Pakistan. *Geol. J.*, **56**, 9, 4760–4778, doi: 10.1002/gj.4209.
- Komadja G. C., Pradhan S. P., Oluwasegun A. D., Roul A. R., Stanislas T. T., Laïbi R. A., Adebayo B., Onwualu A. P., 2021: Geotechnical and geological investigation of slope stability of a section of road cut debris-slopes along NH-7, Uttarakhand, India. *Results Eng.*, **10**, 100227, doi: 10.1016/j.rineng.2021.100227.
- Kumar V., Gupta V., Sundriyal Y. P., 2019: Spatial interrelationship of landslides, lithotectonics, and climate regime, Satluj valley, Northwest Himalaya. *Geol. J.*, **54**, 1, 537–551, doi: 10.1002/gj.3204.
- Lahai Y. A., Anderson K. F. E., Jalloh Y., Rogers I., Kamara M., 2021: A comparative geological, tectonic and geomorphological assessment of the Charlotte, Regent and Madina landslides, Western area, Sierra Leone. *Geoenvironmental Disasters*, **8**, 16, doi: 10.1186/s40677-021-00187-x.
- Liu W., Luo X., Huang F., Fu M., 2017: Uncertainty of the soil–water characteristic curve and its effects on slope seepage and stability analysis under conditions of rainfall using the Markov chain Monte Carlo method. *Water*, **9**, 10, 758, doi: 10.3390/w9100758.
- Loke M. H., Chambers J. E., Rucker D. F., Kuras O., Wilkinson P. B., 2013: Recent developments in the direct-current geoelectrical imaging method. *J. Appl. Geophys.*, **95**, 135–156, doi: 10.1016/j.jappgeo.2013.02.017.
- Lupiano V., Rago V., Terranova O. G., Iovine G., 2019: Landslide inventory and main geomorphological features affecting slope stability in the Picentino River Basin (Campania, southern Italy). *J. Maps*, **15**, 2, 131–141, doi: 10.1080/17445647.2018.1563836.
- Muñoz-Torrero Manchado A., Allen S., Ballesteros-Cánovas J. A., Dhakal A., Dhital M. R., Stoffel M., 2021: Three decades of landslide activity in western Nepal: new insights into trends and climate drivers. *Landslides*, **18**, 6, 2001–2015, doi: 10.1007/s10346-021-01632-6.
- Nakano T., Wada K., Yamanaka M., Kamiya I., Nakajima H., 2016: Precursory slope deformation around landslide area detected by InSAR throughout Japan. *Int. Arch. Photogramm. Remote Sens. Spatial Inf. Sci.*, **XLI-B1**, 1201–1205, doi: 10.5194/isprs-archives-XLI-B1-1201-2016.
- Nepal National Building Code NBC 105 (NBC 105), 2020: Seismic Design of Buildings in Nepal. Department of Urban Development and Building Construction, Kathmandu, Nepal.
- Nepal Red Cross Society, 2003: Disaster preparedness plan. Nepal Red Cross Society.
- Nugraha H., Wacano D., Dipayana G. A., Cahyadi A., Mutaginc B. W., Larasati A., 2015: Geomorphometric characteristics of landslides in the Tinalah watershed, Menoreh Mountains, Yogyakarta, Indonesia. *Procedia Environ. Sci.*, **28**, 578–586, doi: 10.1016/j.proenv.2015.07.068.
- Pokharel B., Thapa P. B., 2019: Landslide susceptibility in Rasuwa District of central Nepal after the 2015 Gorkha Earthquake. *J. Nepal Geol. Soc.*, **59**, 79–88,

- doi: 10.3126/jngs.v59i0.24992.
- Rathore H. A., Niaz A., Farooq M., Khan M. Y., Turab S. A., Saralioglu E., Noor S., Niaz J., 2024: Geophysical and geotechnical characterization of Lower Sudhan Gali Landslide (LSGL), Bagh Azad Jammu & Kashmir. *Geomatics, Nat. Hazards Risk*, **15**, 1, 2383775, doi: 10.1080/19475705.2024.2383775.
- Roback K., Clark M. K., West A. J., Zekkos D., Li G., Gallen S. F., Chamlagain D., Godt J. W., 2018: The size, distribution, and mobility of landslides caused by the 2015  $M_w$ 7.8 Gorkha earthquake, Nepal. *Geomorphology*, **301**, 121–138, doi: 10.1016/j.geomorph.2017.01.030.
- Sassa K., Fukuoka H., Wang F., Wang G., 2007: *Progress in Landslide Science*. Springer Berlin, Heidelberg.
- Segoni S., Pappafico G., Luti T., Catani F., 2020: Landslide susceptibility assessment in complex geological settings: sensitivity to geological information and insights on its parameterization. *Landslides*, **17**, 10, 2443–2453, doi: 10.1007/s10346-019-01340-2.
- Shrestha D., Singh P., Nakamura K., 2012: Spatiotemporal variation of rainfall over the central Himalayan region revealed by TRMM Precipitation Radar. *J. Geophys. Res. Atmos.*, **117**, D22, D22106, doi: 10.1029/2012JD018140.
- Sigdel A., Adhikari R. K., 2020a: Engineering geological and geotechnical studies of Taprang landslide, west-central Nepal: An approach for slope stability analysis. *J. Geol. Res.*, **2**, 4, 22–35, doi: 10.30564/jgr.v2i4.2302.
- Sigdel A., Adhikari R. K., 2020b: Application of Electrical Resistivity Tomography (ERT) survey for investigation of the landslide: a case study from Taprang landslide, Kaski district, west-central Nepal. *J. Nepal Geol. Soc.*, **60**, 103–115, doi: 10.3126/jngs.v60i0.31261.
- Skilodimou H. D., Bathrellos G. D., Koskeridou E., Soukis K., Rozos D., 2018: Physical and anthropogenic factors related to landslide activity in the Northern Peloponnese, Greece. *Land*, **7**, 3, 85, doi: 10.3390/land7030085.
- Stöcklin J., Bhattarai K. D., 1977: *Geology of Kathmandu area and Central Mahabharat range: Nepal Himalaya*. DMG/UNDP Mineral Exploration project, technical report, 86 p. (with 15 maps).
- Summa V., Tateo F., Giannossi M. L., Bonelli C. G., 2010: Influence of clay mineralogy on the stability of a landslide in Plio-Pleistocene clay sediments near Grassano (Southern Italy). *Catena*, **80**, 2, 75–85, doi: 10.1016/j.catena.2009.09.002.
- Upreti B. N., Dhital M. R., 1996: *Landslide Studies and Management in Nepal*. International Centre for Integrated Mountain Development, 87 p.
- Upreti B. N., 2001: The Physiographic and Geology of Nepal and Their Bearing on the Landslide Problem. In: Li T. C., Chalise S. R., Upreti B. N. (Eds.): *Landslide Hazard Mitigation in the Hindu Kush-Himalaya*. International Centre for Integrated Mountain Development, Kathmandu, pp. 31–49.
- Wang H., Zhang L., Luo H., He J., Cheung R. W. M., 2021: AI-powered landslide susceptibility assessment in Hong Kong. *Eng. Geol.*, **288**, 106103, doi: 10.1016/j.enggeo.2021.106103.

- Williams J. G., Rosser N. J., Kinney M. E., Benjamin J., Owen K. J., Densmore A. L., Milledge D. G., Robinson T. R., Jordan C. A., Dijkstra T. A., 2018: Satellite-based emergency mapping using optical imagery: Experience and reflections from the 2015 Nepal earthquakes. *Nat. Hazards Earth Syst. Sci.*, **18**, 1, 185–205, doi: 10.5194/nhess-18-185-2018.
- Xu C., Tian Y., Zhou B., Ran H., Lyu G., 2017: Landslide damage along Araniko highway and Pasang Lhamu highway and regional assessment of landslide hazard related to the Gorkha, Nepal earthquake of 25 April 2015. *Geoenviron. Disasters*, **4**, 14, doi: 10.1186/s40677-017-0078-9.
- Yalcin A., 2011: A geotechnical study on the landslides in the Trabzon Province, NE, Turkey. *Appl. Clay Sci.*, **52**, 1-2, 11–19, doi: 10.1016/j.clay.2011.01.015.
- Zhao Y., Xu M., Guo J., Zhang Q., Zhao H., Kang X., Xia Q., 2015: Accumulation characteristics, mechanism, and identification of an ancient translational landslide in China. *Landslides*, **12**, 6, 1119–1130, doi: 10.1007/s10346-014-0535-4.
- Zhang L. M., Gao L., Zhou S. Y., Cheung R. W. M., Lacasse S., 2017: Stress Testing Framework for Managing Landslide Risks Under Extreme Storms. In: Mikos M., Tiwari B., Yin Y., Sassa K. (Eds.): *Advancing Culture of Living with Landslides*. WLF 2017, Springer, Cham, pp. 17–32, doi: 10.1007/978-3-319-53498-5\_3.